



Deposited via The University of Leeds.

White Rose Research Online URL for this paper:

<https://eprints.whiterose.ac.uk/id/eprint/118288/>

Version: Accepted Version

Article:

Rashid, F, Glover, PWJ, Lorinczi, P et al. (2017) Microstructural controls on reservoir quality in tight oil carbonate reservoir rocks. *Journal of Petroleum Science and Engineering*, 156. pp. 814-826. ISSN: 0920-4105

<https://doi.org/10.1016/j.petrol.2017.06.056>

© 2017 Elsevier B.V. This is an author produced version of a paper published in the *Journal of Petroleum Science and Engineering*. This manuscript version is made available under the Creative Commons Attribution-NonCommercial-NoDerivatives 4.0 International <http://creativecommons.org/licenses/by-nc-nd/4.0/>.

Reuse

Items deposited in White Rose Research Online are protected by copyright, with all rights reserved unless indicated otherwise. They may be downloaded and/or printed for private study, or other acts as permitted by national copyright laws. The publisher or other rights holders may allow further reproduction and re-use of the full text version. This is indicated by the licence information on the White Rose Research Online record for the item.

Takedown

If you consider content in White Rose Research Online to be in breach of UK law, please notify us by emailing eprints@whiterose.ac.uk including the URL of the record and the reason for the withdrawal request.

Microstructural controls on reservoir quality in tight oil carbonate reservoir rocks

Rashid, F.¹, Glover, P.W.J.², Lorinczi, P.², Hussein, D.³, Lawrence, J. A.⁴.

¹ Oil, Gas and Energy Management Department, CANM, Charmo University, Iraq.
Email: fraidoon.rashid@charmouniversity.org, Phone: +9647701924416

² School of Earth and Environment, University of Leeds, UK

³ Geology Department, University of Sulaimani, Iraq.

⁴ Department of Civil and Environmental Engineering, Imperial College London, UK.

Abstract

In carbonate reservoir rocks the complex interaction between the petrophysical properties corresponds to the various depositional microstructures which are modified by various diagenetic processes that ultimately define the reservoir quality, and pose challenges to the prediction of permeability. The permeability heterogeneity in the carbonate oil reservoirs of northern Iraq varies widely and is thought to be controlled by a number of different factors. In this work, controls of matrix permeability for the Cretaceous Kometan formation selected from five oil fields in Kirkuk embayment zone have been investigated. Helium porosity, helium pulse decay permeability, brine permeability, Nuclear Magnetic Resonance (NMR), Mercury Injection Capillary pressure (MICP), Scanning Electronic Microscopy (SEM), X-Ray diffraction (XRD), and photomicrography of thin section have been used to investigate the effect of microstructure on the variation of permeability in the Kometan Formation. The formation has porosities and permeabilities which range from $0.5\pm 0.5\%$ to $29\pm 0.5\%$ and from $0.65\pm 0.08 \mu\text{D}$ to $700\pm 0.08 \mu\text{D}$ respectively. Three types of pore systems have been investigated using pore type, pore size and pore-throat size as characterizing parameters. We have recognized three microstructural types: (i) matrix composed of nano-intercrystalline pores (pore diameter d_p smaller than $1 \mu\text{m}$ and a nanoporous pore-throat size), (ii) matrix composed of micro-intercrystalline pores ($1 < d_p < 10 \mu\text{m}$ with a corresponding micron-scale pore-throat distribution), and (iii) meso-intragranular and moldic pores ($d_p > 10 \mu\text{m}$) also with microporous pore-throat radii. The nano-intercrystalline pore system is common across northern Iraq and represents the effective pore system type in the reservoirs of the Kirkuk embayment zone. For these

1 tight carbonate reservoirs, the mineralogy, especially of quartz and clay minerals (illite
2 and smectite), has little relationship with the measured Klinkenberg-corrected
3 permeability. Consequently, mineralogy is not a useful controlling factor for permeability.
4 Diagenetic processes have altered the depositional texture significantly, resulting in
5 changes to the pore size and pore-throat size distribution and affecting the permeability.
6 In addition the matrix permeability is sensitive to stress, with permeability decreases
7 between -4×10^{-4} mD/psi and -4×10^{-5} mD/psi in the effective stress range from 0 psi to
8 4000 psi. It has been found that of the three microstructure pore types the nano-
9 intercrystalline pore system is more sensitive to increasing effective stress compared to
10 the micro-intercrystalline and meso-intragranular pore systems. Laboratory experiments
11 have shown that stylolisation resulting from regional fluid movements has also affected
12 matrix permeability, with the stylolites acting as barriers to fluid flow and considered to
13 be an important source of tightness of the Kometan formation in the Kirkuk embayment
14 fields.

15

16 **1. Introduction**

17 Many carbonate rocks are complex and heterogeneous over a large scale range due to
18 the intercalation of varied depositional textures and post-depositional diagenetic
19 modification of original rock. The result is a rock of variable reservoir quality, which is a
20 challenge to evaluate, especially if the goal is to predict reservoir permeability
21 (Ehrenberg and Nadeau, 2005; Ehrenberg, 2006, Lucia, 2007; Harris, 2010; Palermo
22 et al., 2010; Ronchi et al., 2010; Rashid et al., 2015a). There are many factors
23 governing the petrophysical properties of carbonates which are essential if conceptual
24 and numerical reservoir models are to be constructed (Briguad et al, 2010).

25 The prediction of most petrophysical properties in carbonate reservoir rocks is
26 problematic. This is especially true of permeability and fluid flow because the carbonate
27 rocks often have heterogeneous grain sizes. Those grain sizes are not related simply to
28 pore and pore-throat neither dimensions nor are they just related to the connectivity of
29 pores, as represented by the cementation exponent m . But they can vary laterally and
30 with depth both at large scales and often changing significantly over small distances as

1 well (Rashid et al., 2015a). This variability is the result of tectonic deformation and
2 diagenesis that has continuously altered the parent reservoir rock properties (Wilson
3 and Evans, 2002; Westphal et al., 2004; Davis et al., 2006; Dou et al., 2011; Rong et al.,
4 2012; Rashid et al., 2015b). The combination of these factors controls the
5 microstructure of the pore system and ultimately dictates the distribution of permeability
6 in the carbonate rocks, and hence affects reservoir potential and individual well
7 productivity (Chalmers, 2012; Haines et al., 2016).

8 Accordingly, prediction and evaluation of the permeability of a carbonate reservoir
9 implies an investigation of the properties of its pore microstructure (Anselmetti and
10 Eberli, 1999; Budd, 2002; Melim et al., 2001; van der Land et al., 2013). Budd (2002) has
11 quantified pore system modifications by integrating cementation and compaction in
12 carbonate grainstones with the aim of evaluating permeability. More recently, Makhloufi
13 et al. (2013) investigated the variation of petrophysical parameters associated with
14 sedimentological and diagenetic changes in tight oolitic limestone, while Haines et al.
15 (2015) documented the evolution of pore systems corresponding to fault damage and
16 the associated diagenesis in carbonate lithologies.

17 The objective of this paper is to characterise the pore system modifications which arise
18 from textural changes in tight carbonate reservoir rocks in the Kirkuk embayment fields,
19 and then to consider the combined effect of these textural modifications on the value
20 and variability of matrix permeability. The second part of this work considers both the
21 sensitivity of the permeability of reservoir rocks to changes in effective stress through its
22 effect on the pore microstructure, as well as the effect of stylolitisation and its control on
23 the spatial and temporal evolution of permeability in unconventional tight carbonate
24 rocks. These results can be applied to subsurface reservoirs to improve reservoir quality
25 predictions especially in the newly discovered oil fields and licensed blocks throughout
26 the region.

27

28

29

1 2. Sampling and methods

2 2.1 Sample provenance

3 This study characterises the pore system modifications which arise from textural
4 changes in tight carbonate reservoir rocks in the Zagros Folded belt oil fields, and then
5 considers their combined effect on matrix permeability and its variability. The second
6 part of this work considers both the sensitivity of the permeability of reservoir rocks to
7 changes in effective stress through its effect on the pore microstructure, as well as the
8 effect of stylolitis and its control on the spatial and temporal evolution of
9 permeability in unconventional tight carbonate rocks. These results can be applied to
10 subsurface reservoirs to improve reservoir quality predictions especially in tight
11 carbonate reservoirs.

12 The Zagros Folded Belt covers the northern part and Kurdistan region of Iraq, and is
13 characterized by the extension of several NE-SW trending structures. The data
14 analysed in this work, including outcrop studies, samples, well cores and logs, were
15 gathered primarily from five oil fields including the Taq Taq, Kirkuk, Jambur, Khabaz
16 and Bai Hassan oil fields ([Figure 1](#)). The Kometan Formation is primarily composed of
17 two beds; a globigerinal limestone (K_1) and a mixed globigerinal/oligostigial limestone
18 (K_2), commonly separated by a glauconitic limestone bed, and a shaly limestone unit
19 which occurs throughout the western part of the zone, especially in the Khabaz and Bai
20 Hassan oil fields ([Figure 2](#)). Throughout most of the Zagros Folded and Thrust belt, the
21 limestone beds of the Kometan Formation are highly stylolitic, compacted, thin and
22 homogenous, while they become non-stylolitic, massive limestone beds towards the
23 western margin of the Zagros Folded belt fields ([Figure 1](#)). The limestone beds of the
24 Kometan Formation are classified as tight carbonate reservoirs ([Rashid et al., 2015a](#)).
25 Their porosity ranges between $0.5\pm 0.5\%$ to $29\pm 0.5\%$, and have permeabilities ranging
26 from $0.65\pm 0.08 \mu\text{D}$ to $700\pm 0.08 \mu\text{D}$. The porosity values in the majority of the studied
27 area do not exceed $10\pm 0.5\%$ with the exception of the Bai Hassan and Khabaz fields,
28 where the porosity increases to $29\pm 0.5\%$.

29 The material collected for analysis in this study included 205 core plug samples
30 representing 99 m of core from one well in each of the 5 fields, as specified in [Table 1](#).

1 Sampling was not necessarily representative of the whole thickness of the formation.
2 The positions of samples were selected based on apparent oil saturation, stylolite
3 distribution, the presence of fractures and lithological variation. All core plugs were
4 nominally 1.5 inches in diameter and 2 inches long. The research materials are
5 summarised in [Table 1](#).

6

Table 1. Core sampling and testing strategy

| Location | Well | Core Length (m) | Core plug numbers | Core measurements number for each analysis type | | | | | | | |
|------------------|-------|-----------------|-------------------|---|----------------------|-------------------------|-----|-----|--------------|-----|------|
| | | | | He Porosity | He Permeability (mD) | Brine Permeability (□D) | SEM | XRD | Thin section | NMR | MICP |
| Taq Taq Field | Tq-1 | 18 | 50 | 50 | 50 | 4 | 2 | 5 | 3 | 10 | 2 |
| Kirkuk field | K-243 | 18 | 61 | 61 | 61 | 4 | 6 | 3 | 4 | 7 | 7 |
| Jambur field | J-37 | 18 | 19 | 19 | 19 | 2 | 3 | 7 | 7 | 10 | 3 |
| Bai Hassan field | BH-13 | 36 | 55 | 55 | 55 | 3 | 9 | 4 | 6 | 15 | 9 |
| Khabaz field | Kz-13 | 9 | 20 | 20 | 20 | 2 | 2 | 4 | 2 | 2 | 2 |

1 2.2 Mineralogy

2 Subsets of 23 samples were selected based on physical appearance, textural change,
3 pore system modifications and gamma ray reflection of the studied intervals. The
4 samples were roughly broken up with a hammer, before being mechanically crushed
5 with a pestle in an agate mortar until they formed powder. A McCrone micronising mill
6 was then used to produce a material with a more uniform grain size, typically 8 µm
7 diameter according to manufacturer's specification after a 12 minute grind. The XRD
8 analysis was carried out on a Philips PW1050 using Cu-K alpha radiation and fitted with
9 a secondary Graphite monochromator. The scan parameter was 3-70 Deg 2 theta, step
10 size of 0.01° and a speed of 0.6°/min.

11

12 2.3 Image analysis

13 22 thin sections, impregnated with Methylene blue dyed epoxy resin, and alizarin red
14 were used to determine the texture, grain type and pore-type distribution. The samples
15 were obtained depending on porosity and permeability relationship and rock texture
16 distribution throughout the studied samples. Thin section photomicrography did not
17 provide effective results for the identification of pore types. Pore types in the sample
18 material were visualized by using high-resolution HRFE-SEM (High resolution field
19 emission scanning electron microscope) with magnifications of 1:10,000 and 1:20,000.
20 A total of 22 samples, 70 mm in size, and with broken surfaces were glued on to
21 aluminium stubs for imaging. The sample material was cleaned using 1% acetic acid
22 solvents to remove any dust or volatile hydrocarbons that may have affected the result,
23 before being coated with a conducting carbon film prior to digital recording of the SEM
24 images.

25 The recorded images were analysed using ImageJ software (thresholding technique).
26 Pore sizes were measured using Feret's diameter ([Ferreira and Rasband, 2012](#)).
27 Multiple measurements of pore sizes were taken for each identified pore on each
28 image. The number of pore size measurement was varied with the amount of pores
29 appeared on each SEM image. An arithmetic mean pore diameter together with a
30 measure of measurement variability was recorded for each sample.

1
2
3
4
5
6
7
8
9
10
11
12
13
14
15
16
17
18
19
20
21
22
23
24
25
26
27
28
29

2.4 Porosity and permeability

A helium gas expansion porosimeter (pycnometer) was used to quantify Helium porosity on the 205 core plugs corresponding to the 99 m of available rock samples. The core plugs were 1.5 inch (38 mm) in diameter and 2.0 inches (51 mm) in length. The estimated porosity can be made to within ± 0.1 porosity unit using the apparatus and protocols at the University of Leeds.

The permeability of cored plug samples was measured using a helium pulse-decay permeameter. This technique works by monitoring the decay of the fluid pressure which is caused by fluid leaking through the sample (Jannot et al., 2007; Zhang et al., 2000; Jones, 1997; Dicker and Smits, 1988; Bourbie and Walls, 1982; Amaefule et al., 1986). Samples were tested at an effective stresses of 800 psi and at four pore fluid pressures (100,150, 200 and 250 psi respectively) in order to calculate the Klinkenberg-corrected permeability for each sample throughout the study area Helium gas . In addition, brine was used for measuring permeability to selected samples for understanding the influence of mineralogy on permeability variation. The composition of the brine was derived from the formation water collected from the studied reservoir in the northern Iraq oil fields as shown on Table (2), (NOC,1987).

To understand the variation of permeability as a function of effective stress, the Klinkenberg-corrected He gas pulse decay permeability was also measured for 9 different effective stress points with confining pressure of 0 to 4000 psi. This procedure was carried out for a subset of 6 samples as it is very time-consuming. The samples were chosen on the basis of their texture, porosity, permeability, pore size, pore throat size and pore types.

The influence of stylolisation on permeability variation throughout tight carbonate rocks was examined in this study. Two sub-sets of stylolitic and non-stylolitic samples of the same well interval and rock textures were selected for permeability measurement. The gas flow movement in this experiment was perpendicular and parallel to the surface of

1 the stylolite's (90° and 0°) using Pulse Decay technique and klinkenberg corrected
2 permeability measurements.

3 **Table 2.** Brine composition used in this study, (NOC, 1987).

| Component | Amount (g/l) |
|-------------------|--------------|
| NaCO ₂ | 0.00521 |
| CaCO ₂ | 0.00077 |
| MgCO ₂ | 0.00023 |
| NaS ₂ | 0.0079 |
| NaCl | 0.01489 |
| Equivalent NaCl | 0.03695 |

4

5 2.5 Mercury Injection capillary pressure (MICP)

6 The mercury injection capillary pressure (MICP) applies pressure up to 60000 psi to
7 calculate pore-throat diameter distribution of the measured sample. The intrusion data
8 were collected using a Micromeritics Autopore IV 9250 apparatus ([Giesche, 2006](#)) for
9 23 samples in this study. Pore system and rock texture distributions were considered for
10 sample selection. The mercury was injected using 62 pressure steps that were
11 distributed logarithmically, and pore-throat size distributions were calculated using the
12 Washburn equation in the usual way ([Washburn, 1921](#); [Webb, 2001](#)).

13 A pore-throat size corresponding to the threshold pressure point on the capillary
14 pressure curve was used as an effective pore throat size that provides a connected
15 pathway to fluid flow through the tight carbonate reservoir samples ([Katz and
16 Thompson, 1987](#)). This value can be used as a convenient parameter for permeability
17 prediction ([Rashid et al., 2015b](#)).

18

19 2.6 Nuclear Magnetic Resonance (NMR) spectroscopy

20

21 The NMR measurements were taken using a Resonance Instruments MARAN 2 bench
22 top spectrometer at atmospheric pressure, 25 °C and 2 MHz. The relaxation time
23 distribution was measured using the MARAN 2 DXP program for 44 samples. Some
24 experimental data about pore size distribution can be obtained from the magnetization

1 modification of water molecules that fill the pore spaces of the analysed samples. The
2 relaxation time T_2 , which is the time of transverse magnetization decay, was measured
3 on each sample. The samples were first saturated with formation water at 1000 psi
4 confining pressure for 24 hours at room temperature in order to fill all their pores with
5 brine, and then the saturated samples were placed in a glass tube which was inserted
6 into the NMR system.

7
8 NMR signals were obtained from the brine when the sample was located in a magnetic
9 field and then excited with a brief pulse of radio frequency energy (Coates et al., 1999).
10 The relaxation time (T_2) provides an efficient signal corresponding to the pore size
11 distribution in porous media. Large pores have longer T_2 values than smaller pores
12 (Westphal et al., 2005; Heath et al., 2011; Al Hinai et al., 2014).

13

14 **3. Results**

15

16 3.1. Mineralogy

17 All samples were predominantly limestone with clay content below 4% except for 2
18 samples which were gathered from the shaly limestone unit, and which have a mean
19 clay content of 49%. The calcium carbonate content of all samples was correspondingly
20 high, usually $\geq 92\%$ throughout the study area, this value reduced to 45% in the shaly
21 limestone samples. Quartz content averaged at about 2% and ranges between zero and
22 4.5%. Illite and smectite dominate the clay content with an average of 1.1 % and ranges
23 between zero and 3.7% without any recording of chlorite and kaolinite clay minerals.
24 Dolomite was identified in some samples taken from Bai Hassan and Khabaz fields. In
25 these fields, a dolomite mineral averages 1.1% with a range between zero and 11%.
26 Pyrite was only observed in one shaly limestone sample (1.1%).

27 3.2 Pore system

28 In this sub-section we describe the pore type, pore size and pore-throat size of the
29 measured samples. Pore types were classified from image analysis based on porosity

1 classification systems of [Choquette and Pray \(1970\)](#). Pore types were subdivided into
2 three classes, derived from depositional and diagenetic modification of rock textural
3 characteristics. The pore types included intercrystalline, moldic and intergranular pores.

4 Pore sizes were sub grouped into three classes: nano-, micro-, and meso-pore sizes.
5 The nano-pore size class includes all pores with a diameter of less than 1 μm . The
6 micro-pore size class includes all pores with a diameter between 1 μm and 10 μm , and
7 the meso-pore size class includes all pores with a diameter greater than 10 μm , and
8 reaching as high as 200 μm . The pore sizes were measured using ImageJ for 22
9 samples, and longitudinal relaxation time distributions (T_2) for 44 samples. The
10 measured pore diameters were used to calibrate the T_2 measurements with the nano-
11 pores having diameters smaller than 1 μm and being associated with short relaxation
12 times, smaller than 100 ms, while micro-pores provided T_2 values greater than 100 ms,
13 and very high relaxation times being observed for moldic and intragranular pores,
14 generally greater than 200 ms. The classification of [Porras and Campos \(2001\)](#) was
15 used to characterise pore-throat sizes derived from MICP analyses with micro-porous
16 textures having pore-throat radii between 0.5 and 0.2 μm , and nano-porous textures
17 being associated with pore-throat radii smaller than 0.2 μm .

18 Three types of pore systems were recognised throughout the studied area, classified by
19 their pore type, pore size and pore-throat size ranges. These are defined in [Table 3](#) and
20 presented in [Figure 3](#). Nano-intercrystalline represents the most common type of pore
21 system throughout the studied samples, covering 80% of the analysis samples. It is
22 characterized by intercrystalline pore types that have nano-scale pore diameter and
23 nano-porous pore throat size. Consequently, 14% of the measured samples referred to
24 the micro-intercrystalline pore system. This pore system is identified from micro-pore
25 size intercrystalline pores that are interconnected by micro-porous pore throat size.
26 Meso-intragranular and moldic pore systems are considered the third type of observed
27 pore system and extended to about 6% of the collected samples. Pore types were
28 dominantly recorded as intragranular and moldic pores with meso-pore size and micro-
29 porous pore throat size.

30

1 **Table 3.** Pore system classifications used in this work.

| Pore Systems | Pore Types | Pore Sizes (μm) | Pore-throat sizes (μm) | NMR T_2 (ms) |
|---------------------------|------------------|-----------------|------------------------|----------------|
| Nano-intercrystalline | Intercrystalline | < 1 | < 0.2 | < 100 |
| Micro-intercrystalline | Intercrystalline | 1 – 10 | 0.2 – 0.5 | 100 – 200 |
| Meso-intragranular/moldic | Intragranular | >10 | > 0.5 | > 200 |

2

3 Nano intercrystalline pore systems are the dominant type in the reservoir samples
 4 studied throughout the oil fields in the Zagros Folded belt.

5

6 3.3 Porosity and permeability

7 Generally, porosity and permeability are positively correlated, and the relationship
 8 between them is a power law (Figure 4). This poroperm diagram, which treats the three
 9 pore types separately, shows measurements of porosity and permeability for the nano-
 10 intercrystalline, micro-intercrystalline and meso-intragranular pore systems respectively.

11 The overall permeability of the reservoir rock is low with values ranging from 65 ± 0.08
 12 nD to $700 \pm 0.08 \mu\text{D}$. The nano-intercrystalline pore system has a porosity ranging from
 13 $0.5 \pm 0.5\%$ to $10 \pm 0.5\%$, and permeabilities which range from $0.65 \pm 0.08 \mu\text{D}$ - $51 \pm 0.08 \mu\text{D}$
 14 (Figure 4; green shading). In micro-intercrystalline pores, porosity is enhanced by
 15 comparison to the nano-intercrystalline pore system, with porosities ranging from
 16 $12 \pm 0.5\%$ to $25 \pm 0.5\%$ and correspondingly larger permeabilities, between $65 \pm 0.08 \mu\text{D}$ to
 17 $600 \pm 0.08 \mu\text{D}$ (Figure 4; blue shading). The third pore system type has porosity greater
 18 than the two previous pore systems. The measured porosity in the meso-
 19 intragranular/moldic pore system ranges from $20 \pm 0.5\%$ to $29 \pm 0.5\%$; and the
 20 permeability lies between $90 \pm 0.08 \mu\text{D}$ and $700 \pm 0.08 \mu\text{D}$ (Figure 4; red shading). The
 21 poroperm statistics for each pore system are presented in Table 4.

1 Anisotropic permeability was examined by carrying out measurements on horizontal and
2 vertical plugs taken from the core samples using pulse decay technique for measuring
3 Klinkenberg corrected permeability. The sample selection procedure was arranged
4 based on matrix texture, and pore system of the rock samples as well as core sample
5 availability. For the Kometan Formation, fluid flow is isotropic at a core-plug scale, with
6 the horizontal and vertical permeabilities showing similar values (Figure 5). The small
7 differences between the vertical and horizontal permeabilities can be ascribed to
8 heterogeneity of the rock texture and sample selection.

9 The porosity and permeability distributions throughout the study area correlate
10 dominantly with diagenetic modification of the rock structure, and this variation causes
11 extensive heterogeneity in reservoir quality. The nano-intercrystalline pore system
12 occurs within the globogerinal limestone (K_1) and mixed globogerinal/oligostiginal
13 limestone (K_2) rock units from the majority of the studied fields in the Kirkuk embayment.
14 This type of pore system has poor reservoir quality because cementation, compaction
15 and stylolisation together reduce reservoir potential. In contrast, the dominant pore
16 types in the western part of the Kirkuk embayment fields are the micro-intercrystalline
17 pore system, which is associated with the globogerinal limestone (K_1), and the meso-
18 intragranular pore system, which was recorded in mixed globogerinal/oligostiginal
19 limestone (K_2) only. In this part of the study area the lack of stylolisation and the effect
20 of dissolution has enhanced reservoir quality, especially porosity and permeability,
21 within the reservoir rock units.

22

23

24

25

26

27

1

2 **Table 4.** Poroperm statistics for the three pore systems.

| Static parameters | Nano-intercrystalline | | Micro-intercrystalline | | Meso-intragranular | |
|--------------------|---------------------------|----------------------------|---------------------------|----------------------------|---------------------------|----------------------------|
| | ϕ (-) ± 0.005 | K (μ D) ± 0.08 | ϕ (-) ± 0.005 | K (μ D) ± 0.08 | ϕ (-) ± 0.005 | K (μ D) ± 0.08 |
| Mean | 0.5 | 7 | 18 | 380 | 23 | 350 |
| Standard deviation | 2 | 8.9 | 16 | 140 | 3 | 170 |
| Mode | 4 | 10 | 19 | 360 | 20 | 310 |
| Median | 5 | 4.1 | 18 | 390 | 22 | 35 |
| Maximum | 10 | 51 | 25 | 600 | 29 | 700 |
| Minimum | 0.5 | 0.65 | 12 | 65 | 20 | 90 |

3

4 **3.4 Permeability sensitivity to effective stress**

The measured samples were selected based on pore system changes throughout the data set. Two samples were taken for each pore system type and submitted to klinkenberg-corrected helium permeametry for 9 confining pressures with a constant pore fluid pressure $p = 100$ psi, resulting in data for 9 effective pressures σ_e (Figure 6) spanning the range 0 psi to 4000 psi. The ranges of confining pressures were chosen according to the reservoir depth of the Kometan formation throughout the studied field.

11 The measured permeability decreases with increasing effective pressure in all cases.
 12 The relationship between the permeability and effective stress is non-linear. We have
 13 fitted exponential curves to the data to account for the non-linear behaviour. This is a
 14 well-recognised pattern (e.g., Chalmers et al., 2012) and is caused by thin-flat high
 15 aspect ratio pores, whatever their size, being more sensitive to closure and closing at
 16 lower effective stresses, with rounder, lower aspect ratio pores remaining until relatively
 17 high effective stresses are attained (Glover et al., 1997; 2000). The closure of the high
 18 aspect ratio pores has a greater effect on measured permeability per unit loss of pore

1 volume because their nature causes them to be more interconnected and their loss
2 reduces the overall permeability by a correspondingly larger amount (Glover et al.,
3 1997; 2000).

4 The low porosity/low permeability nano-intercrystalline pore type is most sensitive to
5 effective stress, following a relationship of the type $k(\sigma_e) = k(\sigma_e = 0)e^{a\sigma_e}$ (Chalmers et
6 al, 2012), where the decay rate a is -4×10^{-4} /psi for Sample 1 and Sample 2. Both
7 samples from the micro-intercrystalline pore type and the two samples from the meso-
8 intragranular pore type also follow the same relationship, but this time with an a -value of
9 about -4×10^{-5} /psi, resulting in a much lower sensitivity to effective stress. The
10 permeability of the nano-intercrystalline pore type decreases by about 400% as the
11 effective stress increases, whilst in the other two pore types it only decreased by about
12 20%.

13

14 3.5 Permeability variation with stylolitization

15 Approximately 8 stylolitic and 16 non-stylolitic core plug reservoir samples were
16 selected from the Bai Hassan and Khabaz oil fields in order to understand the effect of
17 the stylolitization on the fluid flow in the Kometan throughout the studied area. The
18 burial depth of the Kometan Formation is relatively large, varying from 1400 m to
19 2700 m. The loss in primary porosity and matrix permeability by compaction is
20 consequently significant. Chemical compaction which is represented by relative
21 abundance of stylolites is very common in the Kometan reservoir rocks throughout the
22 Kirkuk embayment fields.

23 The limestone beds of the Kometan Formation in the Taq Taq, Kirkuk and Jambur fields
24 are characterized by a great abundance of stylolites. By contrast, the presence of
25 stylolites in the Bai Hassan and Khabaz fields was more limited both in number and
26 distribution. Nevertheless, they all share similar petrophysical properties. Overall, the
27 impact of cementation on the rock fabrics of the Kometan Formation is derived from
28 burial cementation and stylolitization, which exercise a great influence on reservoir
29 quality. There is approximately two orders of magnitude difference between the

1 permeability of samples containing stylolites and those which have no stylolites.
2 Furthermore stylolitic samples also have a matrix pore size which is ten times smaller
3 than comparative non-stylolitic samples, showing that cementation is also occurring
4 away from the stylolite itself. **Figure 7** shows the poroperm diagram for 24 samples that
5 were chosen to study the effects of stylolisation. The rock textures of two highlighted
6 samples both have similar mudstone microstructure. Both the stylotised and non-
7 stylotised samples conform to an approximately linear relationship on this log-log
8 diagram. The samples that have not undergone the formation of stylolites have much
9 higher porosities (10% to 29%) and permeabilities (60 μ D to 0.5 mD) than those
10 containing stylolites, which have porosities in the range 2% to 9% and permeabilities
11 which are also correspondingly low (3 nD -30 μ D).

12 It is clear that the formation of stylolites has reduced any reservoir quality that may have
13 been originally present in the rock, not only because of the formation of the stylolite
14 itself, but due also to associated cementation that reduces the pore size significantly.

15 **4. Discussion**

16 17 4.1. Mineralogy

18 None of the XRD-analyzed samples showed clay volume compositions in excess of 4%
19 and 0% clay volume were recorded in some samples (**Table 1**). If one considers all of
20 the samples then those with the highest and lowest permeabilities contain very similar
21 clay volume compositions. Consequently, it would be reasonable to infer that clay
22 volume composition in the Kometan Formation has no significant effect on permeability.

23 Smectite and illite are the only clay minerals recorded from the XRD analyses. In larger
24 quantities most studies have shown that these clay minerals reduce ([Zhao et al., 2016](#);
25 [Chalmers et al., 2012](#)). In this study, we have not observed any clear relationship
26 between permeability and clay content. Furthermore, we have used brine to measure
27 liquid permeability for selected samples in order to understand impactation of clay
28 contents on permeability and accuracy of measured klinkenberg-corrected helium
29 permeability of the same set of samples, but we have not observed any reaction

1 between the brine and mineralogical composition of the rock samples and changing in
2 the magnitude of brine permeability that possibly happen because of rock-water
3 interaction.

4 All parts of **Figure 8** indicate that while mineralogical changes may have some small
5 control on permeability, there are much stronger influences exercised by the initial
6 depositional texture and diagenetic processes which alter the microstructure of the rock
7 but not its mineralogy.

8 4.2 Initial depositional texture and diagenesis

9 The initial depositional texture can exercise an important control on the initial pore
10 system, defining the porosity and permeability of carbonate rocks (Loucks, 2002; Lucia,
11 1995). The original grainstone texture, characterized by highly interconnected inter-
12 particle macro-pores, has permeability much greater than in packstones and
13 wackstones, which mainly contain micro-pores, together with rarer macro-pores and
14 lime mud. In this study we have not observed any micro- and macro-pores in the
15 globigerinal and oligosteginal wackstone and packstone textures because a range of
16 diagenetic and deformational processes has modified the initial depositional texture.
17 These strong diagenetic influences exercise the dominant control on porosity and
18 permeability. They include compaction (Schmoker and Halley, 1982), consolidation
19 (Rashid et al, 2015 a), stylolitisation (Nelson, 1981; Finkel and Wilkinson, 1990), and
20 cementation (Hollis et al., 2010), which all tend to reduce reservoir porosity and
21 particularly permeability, whilst dissolution (Moore and Druckman, 1981; Ahr and Hull,
22 1983) and dolomitisation can enhance porosity and fluid flow pathways (Al-Qayim and
23 Rashid, 2012). Dissolution, however, often increases porosity with no gross change in
24 permeability because the additional porosity is in the form of isolated pores within a
25 largely unchanged lower permeability matrix. For example, dissolved mudstones have
26 greater magnitude of permeability in comparison with cemented wackstones (**Figure 4**).

27 Hence, the reservoir quality of tight carbonates may be controlled to a small amount by
28 its mineralogy, but the primary control is via the microstructure of the pore system and

1 that is defined by the depositional texture and, importantly, by post-depositional
2 diagenetic processes.

3 4.3. Pore systems

4 Post-depositional diagenetic textural modifications affect permeability by changing the
5 porosity and pore systems connectivity (Glover 2009; Glover et al., 2010). The ability of
6 fluid to flow from one part of the pore structure to another, for any given porosity, is
7 critically controlled by pore size and even more by pore-throat size (Melim et al., 2001;
8 Weger et al., 2009). Here we assess the impact of changing pore sizes and pore-throat
9 sizes on permeability as well as integrating the relationships with other geological
10 parameters in order to understand the evolution of permeability across tight carbonate
11 rocks.

12 It has long been recognised that permeability enhancement in carbonates is controlled
13 by pore size for a given porosity with macro-pore connectivity considered to be the
14 essential factor governing permeability (Melim et al., 2001). In this study, we have not
15 observed any macro-pores within the heterogeneous textures of our samples. By
16 contrast we observe three different pore sizes; nano-pores, micro-pores and meso-
17 pores. The correlation between porosity and permeability in carbonate rocks is
18 commonly poor because of their heterogeneous and complex pore systems (Haines et
19 al., 2016). However, the poroperm relationships of the Kometan Formation samples
20 show a clear positive correlation ($R^2 = 0.70$) between measured porosity and
21 permeability (Figure 4).

22 The correlation between the magnitudes of the measured Klinkenberg-corrected
23 permeabilities and pore sizes for the 22 samples for which we made pore size
24 measurements using Feret's diameter method (Ferreira and Rasband, 2012) is
25 presented in Figure 9. Comparing the nano-intercrystalline and micro-intercrystalline
26 samples, it can be seen that an increase of about one order of magnitude in pore
27 diameter is associated with a 2 to 3 order of magnitude increase in permeability. This is
28 approximately compatible with the range of permeability prediction models that were
29 primarily designed for clastic rocks where the permeability scales as the square of the

1 grain size (and hence the pore size and pore-throat size) (Glover et al., 2006 Swanson,
2 1981, and Van Baaren, 1979). However, the pattern between the micro-intercrystalline
3 and meso-intergranular is different. One would expect a further increase in permeability
4 by perhaps one order of magnitude to be associated with a fourfold increase in pore
5 throat diameter, but instead there is a slight decrease in permeability. This may be
6 caused by the pore diameter measurement being dominated by a few large pores that
7 remain isolated within the matrix, and consequently do not contribute to any increase in
8 permeability. These large pores are associated with the presence of foraminifer moulds
9 (*globigerina* and *oligostegina* chambers). The decrease in permeability that is observed
10 is not explained and could be due to the restricted dataset of only 3 samples.. This
11 unexpected increase in permeability associated with an increase in porosity is a very
12 significant observation in carbonate rocks and underlines the heterogeneous
13 microstructure of carbonates and its complex relationship with permeability and porosity
14 (Rezaee et al., 2007 , Palermo et al., 2010, Makhloufi et al, 2013 , and Rashid et al.,
15 2015a; 2015b).

16 Unlike conventional carbonate reservoir rocks, tight carbonates are characterized by
17 nanometer scale pore-throat sizes (diameters) that provide poor connectivity. Two pore-
18 throat size classes were investigated throughout this research (Table 3). Figure 10
19 presents a correlation between the magnitudes of the measured Klinkenberg-corrected
20 permeabilities and pore-throat size, with pore-throat size obtained from the pore
21 diameter corresponding to the threshold pressure point on the capillary pressure curve
22 (Katz and Thompson, 1987).

23 It is immediately clear that the majority of the data are described well by a relationship
24 where the permeability depends on the square of the pore throat size $k = 2.1979 \times d_{PT}^{2.0071}$.
25 Perhaps this should not be surprising as the SI units for permeability are length
26 squared. In fact, there are many equations for the prediction of permeability in clastic
27 rocks which include the length squared term. A review of many of them can be found in
28 either Glover et al. (2006) or Rashid et al. (2015b). That we find a squared relationship
29 when comparing permeability as a function of pore throat size, is interesting because
30 not only does it imply that tight carbonate rocks share some of the microstructural

1 physics that we applied to clastic rocks, it also implies that there is some linear
2 relationship between pore throat size, pore size, and grain size in tight carbonates, i.e.,
3 $d_{PT} \sim d_{Pore} \sim d_{grain}$.

4 4.4. Effective stress

5 Understanding of the sensitivity of permeability to variations in effective stress is
6 considered to be essential in assessing production from a reservoir rock because pore
7 pressure decreases with production rate and results in an increase in effective stress
8 (Chalmers et al., 2012). Consequently, the initial reservoir permeability is controlled by
9 how the rock microstructure is affected by burial depth, but the sensitivity of the
10 reservoir permeability to change as the reservoir is produced and as the effective
11 pressure increases depends on how sensitive the microstructure of the rock is to
12 changes in effective pressure (Byrnes and Keighin, 1993, Byrnes, 1997 and Ghabezloo
13 et al., 2008), and that microstructure sensitivity can be anisotropic and mineralogy-
14 dependent (Chalmers et al., 2012).

15 While the variability of permeability with effective stress can be direction-dependent,
16 measurements of vertical and horizontal permeability in the Kometan Formation have
17 shown that the hydraulic conductivity of the horizontal and vertical flows is similar
18 (Figure 6). Whatever small differences exist in the magnitude of the vertical and
19 horizontal permeabilities are probably derived from heterogeneity of the rock texture
20 and sample selection. Based on this result we expect the sensitivity of permeability to
21 effective stress to be the same both vertically and horizontally to the bedding. In other
22 words, we expect the vertical and horizontal permeability have the same sensitivity of
23 variation as function of applied stress.

24 Due to the sensitivity of the nano-intercrystalline pore system samples were of low
25 reservoir quality, this would be exacerbated when trying to produce from this pore
26 system by further reductions in permeability. The main differences in the sensitivity
27 between the nano intercrystalline and the other 2 pore system type's shows that the
28 stress sensitivity of permeability is strongly controlled by the rock microstructure, which
29 is a result of diagenetic modification, especially modifications that alter the pore-throat

1 size. Nano-porous pore throats are dominantly sensitive to applied stress in comparison
2 to micro-porous throats. Thus, permeability of the highly compacted and cemented rock
3 structures (nano-intercrystalline pore system) decreased more than other pore system
4 once stress was applied. This conclusion is derived from the microstructures and pore
5 system anisotropy throughout the reservoir rocks. The Nano-intercrystalline pore
6 system has considerable contrast between grain sizes and pore sizes, the rock matrix
7 have a grain size greater than 200 μm , while pore sizes are smaller than 1.0 μm and
8 pore throat sizes smaller than 0.1 μm . Any increasing of applied stress compresses
9 available spaces between the matrix grains especially when compared with the two
10 other pore systems. The micro-intercrystalline pore system and meso-intragranular pore
11 system average pore systems are 10 μm and 100 μm respectively.

12 Consequently, the permeability of Kometan reservoirs in the Bai Hassan and Khabaz
13 fields is less likely to be affected by stress sensitivity than of permeability into account,
14 there is less risk associated with Kometan reservoirs in the Bai Hassan and Khabaz
15 fields in comparison with the fields located in the Kirkuk embayment or recently
16 discovered fields and licensed Kurdistan licensed blocks where the Kometan reservoirs
17 are more sensitive to stress changes (Kirkuk (Baba dome), Jambur and Taq Taq fields).

18

19 4.4. Stylolisation

20 The impact of stylolisation on permeability and regional fluid flow is considered as a
21 crucial point in petroleum exploration. Stylolites and reprecipitation derived from
22 stylolisation have been identified as dominant destructive factors on reservoir quality.
23 The stylolites decrease porosity and permeability of the parent rocks, and have been
24 investigated as a fluid flow barriers in several reservoir rocks (Nelson, 1981; Burgess
25 and Peter, 1985; Koepnick, 1987; Finkel and Wilkinson, 1990; Dutton and Willis, 1998;
26 Alsharhan and Sadd, 2000). By contrast, several researches have concluded that this
27 type of deformation can enhance reservoir potential (Dawson, 1988; Raynaud and
28 Carrio- Schaffhauser, 1992; Van Geet et al., 2000; Gingras et al., 2002; Harris, 2006;
29 Heap et al, 2014).

1 In this work, we have already recognised that non-stylolite and stylolite samples have
2 very significantly different power law permeability-porosity relationships (Figure 7). We
3 can say with certainty that in the Kometan Formation stylolites act as barriers to fluid
4 flow. In these rocks reprecipitated calcium carbonate occludes pores and pore throats
5 reducing connectivity considerably. In addition, data from XRD measurements have
6 shown that the volume of CaCO₃ in stylolitic samples is greater than that in non-stylolitic
7 samples by 7%, and we ascribe that increase to the additional calcite cementation
8 associated with stylolitisation. Consequently, we consider the tightness of the Kometan
9 reservoir throughout the majority of the Kirkuk embayment and other parts of the Zagros
10 Fold-Thrust belt has resulted from stylolitisation which is regionally distributed.

11

12 **5. Conclusions**

13 In this study, 205 core plugs samples were collected from the Cretaceous Kometan
14 Formation in hydrocarbon bearing zone throughout the Kirkuk embayment, Zagros
15 Folded Zone and oil fields for petrophysical, petrographical and mineralogical analysis.
16 The relationships between the mineralogy, texture, pore system, stylolitisation and
17 effective stress variation with permeability were examined, leading to the following
18 conclusions.

- 19 1. The original rock textures should not be considered as the single important factor
20 controlling the permeability potential in tight carbonate reservoir rocks because
21 diagenetic modification has significantly changed the depositional rock structure.
22 The resulting pore system has often undergone compaction, consolidation,
23 cementation, and stylolitisation reducing porosity and permeability as well as
24 dissolution and dolomitisation which may enhance porosity and permeability.
- 25 2. Increasing volumes of clays and quartz have only a minor impact on permeability
26 in these tight carbonate rocks.
- 27 3. Increased permeability in these tight carbonate reservoir rocks is associated with
28 good pore connectivity that occurs in rocks with micro-intercrystalline and meso-
29 intragranular pore types. The fluid flow is controlled by pore-throat sizes greater
30 than 0.1 µm.

- 1 4. Nano-intercrystalline pore systems represent the most common pore system in
2 the Kometan Formation. This pore system has permeability which is more
3 sensitive to changes in effective stress than the other 2 types of pore system.
4 Consequently there is a higher production risk associated with reservoirs
5 composed predominantly of this type of pore system as the pore pressures
6 decline during production. The Taq Taq, Kirkuk (Baba dome), and Jambur fields
7 as well as the Kurdistan region licensed blocks would fall into this category. By
8 contrast, the Khabaz and Bai Hassan oil fields are predominantly composed of
9 the 2 other types of pore system, and hence do not share the same production
10 risk.
- 11 5. Abundant stylolites within the Kometan limestones in the Kirkuk embayment act
12 as barriers to fluid flow and reduce the permeability of the reservoir rocks
13 throughout the region. Stylolite and calcite cementation not only provides an
14 obstacle for regional oil migration but also reduces reservoir potential.

17 **Acknowledgements**

18 We would like to thank Ministry of higher education of Kurdistan region-Iraq government
19 for their financial support of this study with in HCDP scholarship. We would also like to
20 thanks North oil company – Iraq (Kirkuk) for access to core plugs. This work was carried
21 out in The University of Leeds Petrophysics Laboratory and The Wolfson Multiphase
22 Flow Laboratory.

25 **References**

26
27 Ahr , W.M. and Hull, H.B. , 1983 . Burial diagenesis and reservoir development in the
28 North Haynesville (Smackover) Field, Louisiana . Trans. Gulf Coast Assoc. Geol. Soc.
29 v.33 , p.1 – 9 .

- 1 Al Hinai, A., Rezaee, M.R., Esteban ,L., and Labani, M.M., 2014. Comparisons of pore
2 size distribution: A case from the Western Australian gas shale formations, Journal of
3 Unconventional Oil and Gas Resources. v.8, p.1-13.
- 4 Al-Qayim, B., and Rashid, F., 2012. Reservoir characteristics of the albian upper
5 qmachuqa formation carbonates, Taq Taq oil field, Kurdistan, Iraq. Journal of Petroleum
6 Geology, v.35, no.4, p.317-341.
- 7 Alsharhan A. and Sadd J.L., 2000. Stylolites in Lower Cretaceous carbonates
8 reservoirs, U.A.E: Society for Sedimentary Geology Special Publication, v. 69, p.185–
9 207.
- 10 Amaefule, J.O., Wolfe, K., Walls, J.D., Ajufo, A.O., and Peterson, E., 1986. Laboratory
11 determination of effective in low-quality reservoir rocks by the pulse decay technique.
12 SPE15149.
- 13 Anselmetti, F.S., and Eberli, G.P., 1999. The velocity-deviation Log : a tool to predict
14 pore type and permeability trends in carbonate drill holes from sonic and porosity or
15 density Logs, AAPG Bulletin, v.83 ,p.450–466.
- 16 Bourbie, T., and Walls, J., 1982. Pulse Decay Permeability: Analytical Solution and
17 Experimental Test. Journal of Society of Petroleum Engineering, p. 719-721.
- 18 Brigaud B., Vincent B., Durllet C., Deconinck J.F., Blanc P., and Trouiller A., 2010.
19 Acoustic properties of ancient shallow-marine carbonates: effects of depositional
20 environments and diagenetic processes (Middle Jurassic, Paris Basin, France),
21 J. Sediment. Res., v. 80, p.791–807.
- 22 Budd, D.A., 2002. The relative roles of compaction and early cementation in the
23 destruction of permeability in carbonate grainstones: a case study from the Palaeogene
24 of West-Central Florida, USA, Journal of Sedimentary Reservoir, v. 72 ,p. 116–128.
- 25 Burgess C.J., and Peter C.K., 1985. Formation, distribution, and prediction of stylolites
26 as permeability barriers in the Thamama Group, Abu Dhabi: Middle East Oil Technical
27 Conference and Exhibition, 11–14 March 1985, Bahrain.

- 1 Byrnes, A.P., 1997. Reservoir characteristics of low-permeability sandstones in the
2 Rocky Mountains. *The Mountain Geologist*, v.34, p.39-51.
- 3 Byrnes, A.P., and Keighin, C.W. , 1993. Effect of confining stress on pore throats and
4 capillary pressure measurements, selected sandstone reservoir rock, AAPG annual
5 convention program, April 25-28, New Orleans, p.82.
- 6 Chalmers, G.R.L., Ross, D.J.K., and Bustin, R.M. , 2012. Geological controls on matrix
7 permeability of Devonian Gas Shale in the Horn River and Liard basins, northeastern
8 British Columbia, Canada, *International Journal of Coal Geology*, v.103, p.120-131.
- 9 Choquette, P.W., and Pray, L.C., 1970. Geological nomenclature and classification of
10 porosity in sedimentary carbonates. *AAPG Bull.* v.54, no.2, p.207–250.
- 11 Coates, G.R., Xiao, L.Z., and Prammer, M.G., 1999. *NMR Logging: Principles and
12 Applications*, p.234, Houston, USA, Halliburton Energy Services.
- 13 Davis, J.M., Roy, N.D. Mozley, P.S., and Hall, J.S., 2006. The effect of carbonate
14 cementation on permeability heterogeneity in fluvial aquifers: an outcrop analog study,
15 *Sedimentary Geology*, v.184, p. 267–280.
- 16 Dawson W.C., 1988. Stylolite porosity in carbonate reservoirs, *American Association of
17 Petroleum Geologists Search and Discovery Article*, American Association of Petroleum
18 Geologists Annual Convention, Houston, Texas, 20–23March 1988, Article #91030.
- 19 Dicker, A.J., and Smits, R.M., 1988. A practical approach for determining permeability
20 from laboratory pressure-pulse decay measurements. SPE 17578.
- 21 Dou, Q., Sun, Y., and Sullivan, C., 2011. Rock-physics-based carbonate pore type
22 characterization and reservoir permeability heterogeneity evaluation, Upper San Andres
23 reservoir, Permian Basin, west Texas, *journal of applied Geophysics.*, v.74 ,p. 8–18.
- 24 Dutton S.P., and Willis B.J., 1998. Comparison of outcrop and subsurface sandstone
25 permeability distribution, Lower Cretaceous Fall River Formation, South Dakota and
26 Wyoming: *Journal of Sedimentary Research*, v. 68, p. 890–900.

- 1 Ehrenberg, S.N., and Nadeau, P.H., 2005. Sandstone vs. carbonate petroleum
2 reservoirs: A global perspective on porosity-depth and porosity permeability
3 relationships. AAPG Bulletin, v. 89, no. 4, p 435–445.
- 4 Ehrenberg, S.N., 2006. Porosity Destruction in Carbonate Platforms: Journal of
5 Petroleum Geology, v. 29, p. 41-52.
- 6 Ferreira, T., and Rasband, W.S., 2012. Image J user guide, IJ1.46r, revised edition.
- 7 Finkel E.A., and Wilkinson B.H., 1990. Stylolitization as source of cement in
8 Mississippian Salem Limestone, west-central Indiana: AAPG Bulletin, v. 74, p. 174–186.
- 9 Ghabezloo, S., Sulem, J., Guedon, S., Martineau, F., 2008. Effective stress law for the
10 permeability of a limestone. International Journal of Rock Mechanics and Mining
11 Science.
- 12 Giesche, H., 2006. Mercury Porosimetry: A general (practical) overview. Particle &
13 particle systems characterization. v.23, p.9-19.
- 14 Gingras M.K., MacMillan B., Balcom B.J., 2002. Visualizing the internal physical
15 characteristics of carbonate sediments with magnetic resonance imaging and
16 petrography: Bulletin of Canadian Petroleum Geology, v. 50, p. 363–369.
- 17 Glover, P.W.J., and Déry, N., 2010. Streaming potential coupling coefficient of quartz
18 glass bead packs: dependence on grain diameter, pore size, and pore throat radius.
19 Geophysics, v. 75, F225–F241 .
- 20 Glover, P.W.J., and Walker, E., 2009. Grain-size to effective pore-size transformation
21 derived from electrokinetic theory. Geophysics, v. 74, E17–E29.
- 22 Glover, P.W.J., Gómez, J.B. and Meredith, P.G., 2000. Fracturing in saturated rocks
23 undergoing triaxial deformation using complex electrical conductivity measurements:
24 Experimental study. Earth and Planetary Science Letters, v.183, p. 201-213.
- 25 Glover, P.W.J., Gómez, J.B., Meredith, P.G., Hayashi, K., Sammonds, P.R. and Murrell,
26 S.A.F., 1997. Damage of saturated rocks undergoing triaxial deformation using complex

- 1 electrical conductivity measurements: Experimental results. *Physics and Chemistry of*
2 *the Earth*, v.22, p. 57-61.
- 3 Glover, P.W.J., Zadjali, I.I. and Frew, K.A., 2006. Permeability prediction from MICP and
4 NMR data using an electrokinetic approach. *Geophysics*, v.71, p.F49-F60.
- 5 Haines T. J., Michie E.A.H, Neilson J.E., Healy D., 2016. Permeability evolution across
6 carbonate hosted normal fault zones, *Marine and Petroleum Geology*, v. 72, p.62-82.
- 7 Haines, T.J., Neilson, J.E., Healy, D., Michie, E.A.H., and Aplin, A.C., 2015. The impact
8 of carbonate texture on the quantification of total porosity by image analysis, *Computers*
9 *and Geoscience*, v.85, p. 112–125.
- 10 Harris P.M., 2010. Delineating and quantifying depositional facies patterns in carbonate
11 reservoirs: Insight from modern analogs, *AAPG Bulletin*, v.94, no. 1 , p. 61–86.
- 12 Harris N.B., 2006. Low-porosity haloes at stylolites in the feldspathic Upper Jurassic Ula
13 sandstone, Norwegian North Sea: An integrated petrographic and chemical mass-
14 balance approach: *Journal of Sedimentary Research*, v. 76, p.444–459.
- 15 Heap, M.J., Baud P., Reuschlé T., and Meredith P. G.,2014 , Stylolites in limestones:
16 Barriers to fluid flow, *Geology* , v.42, no.1 , p.51-54.
- 17 Heath, J.E., Dewers T.A., McPherson B.J.O.L., Petrusak R., Chidsey T.C., Rinehart
18 A.J., and Mozley P.S., 2011. Pore networks in continental and marine mudstones:
19 characteristics and controls on sealing behaviour, *Geosphere*, v. 7 , p. 429–454.
- 20 Hollis, C., Vahrenkamp, V., Tull, S., Mookerjee, A., Taberner, C., Huang, Y., 2010. Pore
21 system characterisation in heterogeneous carbonates: An alternative approach to w
22 idely-used rock-typing methodologies. *Marine and Petroleum Geology*. v.27, no. 4, p.
23 772-793.
- 24 Jannot, Y., Lasseux, D., Vizé, G., and Hamon, G., 2007. A detailed analysis of
25 permeability and Klinkenberg coefficient estimation from unsteady-state pulse-decay or
26 draw-down experiments. Paper no. SCA2007-08.

- 1 Jones, S.C.,1997. A Technique for Faster Pulse-Decay Permeability Measurements in
2 Tight Rocks.
- 3 Katz, A.J. and Thompson, A.H., 1986. Quantitative prediction of permeability in porous
4 rock. *Physical Review B*, v.34, p.8179-8181.
- 5 Koepnick R.B., 1987, Distribution and permeability of stylolite-bearing horizons within a
6 Lower Cretaceous carbonate reservoir in the Middle East:Society of Petroleum
7 Engineers Formation Evaluation, v. 2.
- 8 Loucks, R.G. , 2002.Controls on reservoir quality in platform-interior limestones around
9 the Gulf of Mexico : example from the lower Cretaceous Pearsall formation in South
10 Texas depositional setting and systems of the Pearsall formation, *Gulf Coast Assoc.*
11 *Geol. Soc. Trans.*, v.52 , p. 659–672.
- 12 Lucia, F.J., 1995, Rock-fabric/petrophysical classification of carbonate pore Space for
13 reservoir characterization, *AAPG Bulletin.*, v.79, p. 1275–1300.
- 14 Lucia, F.J., 2007 .Carbonate Reservoir Characterization: an Integrated Approach,
15 (second edition) Springer (2007).
- 16 Makhloufi Y. , Collin P., Bergerata F., Casteleyn, L. , Claes, S., David, C.,
17 Menendez B., Monnae F., Robion P. , Sizun J., Swennend R., and Rigollet C.,
18 2013 . Impact of sedimentology and diagenesis on the petrophysical properties of a tight
19 oolitic carbonate reservoir. The case of the Oolithe Blanche Formation (Bathonian, Paris
20 Basin, France), *Marine and Petroleum Geology*, v. 48, p.323–340.
- 21 Melim L.A., Anselmetti F.S., and Eberli G.P., 2001. The importance of pore type on
22 permeability of Neogene carbonates, Great Bahama Bank Subsurface Geology of a
23 Prograding Carbonate Platform Margin Great Bahama Bank Results of the Bahamas
24 Drilling Project, *SEPM Special Publication*, p. 217–238.
- 25 Moore, C.H. and Druckman , Y. , 1981 . Burial diagenesis and porosity evolution, Upper
26 Jurassic Smackover, Arkansas and Louisiana. *AAPG Bulletin*, v. 65, p. 597 – 628.

- 1 Nelson R.A., 1981. Significance of fracture sets associated with stylolite zones: The
2 American Association of Petroleum Geologists Bulletin, v. 65, p. 2417–2425.
- 3 North Oil Company ,1987. Final well report , Taq Taq oil field.
- 4 Palermo, D., Aigner, T., Nardon, S., and Blendinger, W.,2010. Three-dimensional
5 facies modeling of carbonate sand bodies: outcrop analog study in an epicontinental
6 basin (Triassic, southwest Germany), AAPG Bulletin, v.94 , p. 475–512.
- 7 Porras, J., and Campos, O., 2001. Rock Typing: A Key Approach for Petrophysical
8 Characterization and Definition of Flow Units, Santa Barbara Field, Eastern Venezuela
9 Basin, SPE 69458, SPE Latin American Conference, Buenos Aires, Argentina..
- 10 Rashid, F., Glover, P.W.J., Lorinczi, P., Hussein, D., Collier, R, 2015b. Permeability
11 prediction in tight carbonate rocks using capillary pressure measurements, marine and
12 petroleum geology, v.68 Part A, p.536-550.
- 13 Rashid, F., Glover, P.W.J., Lorinczi, P., Collier, R., and Lawrence, J., 2015a. Porosity
14 and permeability of tight carbonate reservoir rocks in the north of Iraq. Journal of
15 Petroleum Science and Engineering, v.133, p.147-161.
- 16 Raynaud, S., and Carrio-Schaffhauser E., 1992. Rock matrix structures in a zone
17 influenced by a stylolite: Journal of Structural Geology, v.14, p.973–980.
- 18 Rezaee, M.-R., Motiei , H., and Kazemzadeh, E., 2007. A new method to acquire m
19 exponent and tortuosity factor for microscopically heterogeneous carbonates, Journal of
20 Petroleum Science and Engineering, v. 56, p. 241–251.
- 21 Ronchi P., Giulio A. Di, Ceriani A., and Scotti P., 2010. Contrasting fluid events giving
22 rise to apparently similar diagenetic products; late-stage dolomite cements from the
23 Southern Alps and central Apennines, Italy, Geological Society of London, Special
24 Publications, v. 329, p. 397–413.
- 25 Rong, H., Jiao, Y., Wu ,L., Gu, Y., Zhang, L., Li ,R., and Zeng ,F.,2012. Effects of
26 diagenesis on the acoustic velocity of the Triassic oolitic shoals in the Yudongzi outcrop

- 1 of Erlangmiao area, Northwest Sichuan Basin, *Journal of Earth Science*, v.23, p. 542–
2 558.
- 3 Schmoker, J. W. and Halley, R. B. , 1982. Carbonate porosity versus depth; a
4 predictable relation for South Florida. *AAPG Bulletin.*, v.66, p.2561 – 2570.
5
- 6 Sella, G.F., Dixon, T.H. and Mao, A., 2002. REVEL: A model for recent plate velocities
7 from space geodesy. *Journal of Geophysical Research*, v. 107, no. B4, 2081, p. 30.
- 8 Swanson, B. F., 1981, A simple correlation between permeabilities and mercury
9 capillary pressures: *Journal of Petroleum Technology*, v.33, p.2498– 2504.
- 10 Van Baaren, J.P., 1979, Quick-look permeability estimates using sidewall samples and
11 porosity logs: *Transactions of the 6th Annual European Logging Symposium, Society of*
12 *Petrophysicists and Well Log Analysts*, p.19–25.
- 13 Van der Land, C., Wood, R., Wu, K., van Dijke, M.I.J., Jiang, Z., Corbett, P.W.M., and
14 Couples, G., 2013. Modelling the permeability evolution of carbonate rocks, marine and
15 petroleum geology, v. 48, p. 1–7.
- 16 Van Geet, M., Swennen R., and Wevers M., 2001. Towards 3-D petrography:
17 Application of microfocus computer tomography in geological science: *Computers and*
18 *Geosciences*, v. 27, p. 1091–1099.
- 19 Washburn, E. W., 1921. The Dynamics of Capillary Flow. *Physical Review*, v.17, p.273-
20 283.
- 21 Webb, P. A., 2001. An Introduction to the physical characterization of materials by
22 mercury intrusion porosimetry with emphasis on reduction and presentation of
23 experimental data. Norcross, Georgia.
- 24 Weger, R.J., Eberli G.P., Baechle G.T., Massaferro J.L., and Sun Y.-F., 2009.
25 Quantification of pore structure and its effect on sonic velocity and permeability in
26 carbonates, *AAPG Bulletin.*, v.93, p. 1297–1317

- 1 Westphal, H., Eberli, G.P., Smith, L.B., Grammer, G.M., and Kislak, J., 2004. Reservoir
2 characterization of the Mississippian Madison Formation, Wind River basin, Wyoming,
3 AAPG Bulletin, v. 88, p. 405–432.
- 4 Westphal, H., Surholt, I., Kiesl, C., Thern, H.F. and Kruspe, T., 2005. NMR
5 Measurements in Carbonate Rocks: Problems and an Approach to a Solution. Pure and
6 Applied Geophysics, v.162, p.549-570.
- 7 Wilson, M.E.J. and Evans, M.J., 2002. Sedimentology and diagenesis of Tertiary
8 carbonates on the Mangkalihat Peninsula, Borneo: implications for subsurface reservoir
9 quality. Marine and petroleum geology, v.19,p.873-900.
- 10 Zebari, M., 2013 .Geometry and Evolution of Fold Structures within the High Folded
11 Zone: Zagros Fold-Thrust Belt, Kurdistan region-Iraq, published MSc thesis, University
12 of Nebraska.
- 13 Zebari, M., and Burberry, C.M., 2015. 4-D evolution of anticlines and implications for
14 hydrocarbon exploration within the Zagros Fold-Thrust Belt, Kurdistan Region, Iraq.
15 GeoArabia; Gulf PetroLink, Bahrain, v.20, p.161-188.
- 16 Zhang, M., Takahashi, M., Morin, R. H. and Esaki, T., 2000. Evaluation and Application
17 of the Transient-Pulse Technique for Determining the Hydraulic Properties of Low-
18 Permeability Rocks – Part 1: Theoretical Evaluation. American Society for Testing and
19 Materials : Geotechnical Testing Journal, p.83-90.
- 20 Zhao, H., Ning, Z., Zhao, T., Zhang, R., Wang, Q., 2016. Effects of mineralogy on
21 petrophysical properties and permeability estimation of the Upper Triassic Yanchang
22 tight oil sandstones in Ordos Basin, Northern China, Fuel, v. 186, p. 328-338.

23

24 **Figures titles**

25 **Figure 1.** Physiographic map of the Zagros showing main subdivisions segments of the
26 belt, and highlights oil fields and wells used in this study (Core sampling and testing
27 strategy after Sella et al., 2002; Zebari M., 2013; Zebari M. M. and Burberry C. M.
28 2015).

1

2 **Figure 2.** Two typical sedimentary logs of the Kometan Formation throughout the study
3 area calibrated with the gamma ray deflection. The rock textures are classified as
4 Globigerinal wackstone/packstone limestone (GWP), globigerinal and oligosteginal
5 wackstone/packstone textures (GOWP) and globigerinal mudstone (GM). (A) Well
6 representing the Bai Hassan field, (B) well representing the Taq Taq field.

7

8 **Figure 3.** Pore system types were investigated throughout the studied samples. Nano
9 intercrystalline pore system; A1: SEM micrography shows intercrystalline pores size
10 smaller than 1 μm , A2: Pore size distribution obtained from image analysis, A3: NMR T2
11 spectra < 100 ms, A4: MICP pore throat size distribution < 0.1 μm . Micro intercrystalline
12 pore system; B1: SEM micrography shows intercrystalline pores size larger than 1 μm ,
13 B2: Pore size distribution achieved from image analysis , B3: NMR T2 spectra > 100
14 ms, B4: MICP pore throat size distribution < 0.2 μm . Meso intragranular and moldic pore
15 system; C1: SEM micrography shows intragranular and moldic pores size larger than
16 10 μm , C2: Pore size distribution measured from image analysis, C3: NMR T2 spectra
17 > 200 ms, C4: MICP pore throat size distribution < 0.2 μm .

18

19 **Figure 4.** The relationship between porosity (helium) and permeability (helium,
20 Klinkenberg-corrected) for the samples measured in the Kometan Formation. A:
21 Photomicrograph of polarizing microscope thin section images impregnated with blue
22 epoxy. The traces of blue hue in intercrystalline pores show it has a mudstone texture
23 with a porosity of 0.1876 and a permeability of 0.50 mD. B: Photomicrograph of
24 polarizing microscope thin section images impregnated with blue epoxy, does not show
25 any traces of blue hue pores, it has a wackstone texture with a porosity of 0.032 and a
26 permeability of 0.018 mD permeability.

27

28 **Figure 5.** Measured vertical helium permeability as a function of the measured
29 horizontal helium permeability (both klinkenberg-corrected) for 16 selected samples
30 from the available core data.

31

32 **Figure 6.** The effect of confining pressure (effective, psi) on the magnitude of
33 permeability for two samples for each of the three recognized pore types:

34 The Nano-intercrystalline pore system: A1: SEM micrography shows intercrystalline
35 pores size smaller than 1 μm , A2: Photomicrograph of polarizing microscope thin
36 section image shows wackstone texture. A3 Samples 1 and 2: Permeability variation of
37 these samples as function of effective stress.

1 The Micro-intercrystalline pore system; B1: SEM micrography shows intercrystalline
2 pores size greater than 1 μm , B2: Photomicrograph of polarizing microscope thin
3 section image shows mudstone texture. B3 samples 3 and 4: Permeability variation of
4 these two samples as function of effective stress.

5 The Meso-intragranular pore system; C1: SEM micrography shows intragranular pores
6 size greater than 10 μm , C2: Photomicrograph of polarizing microscope thin section
7 image shows wackstone texture contains blue traced intragranular pores. C3 samples 5
8 and 6: Permeability variation of selected samples as function of effective stress.

9

10 **Figure 7.** Log–log plot of Klinkenberg-corrected helium permeability as a function of
11 helium porosity for a subset of 24 samples measured in this study (measured under at
12 ambient conditions). The dashed lines correspond to power law fits through the stylolitic
13 (red line, red symbols) and the non-stylolitic samples (green line, green symbols). Two
14 highlighted samples represent mudstone rock texture for both stylolitic and non-stylolitic
15 samples.

16

17 **Figure 8.** Effects of mineralogy on permeability in tight carbonate rocks; A1:
18 Klinkenberg-corrected Permeability as a function of Illite-smectite % volume, and A2:
19 brine permeability as a function of Illite-smectite % volume. B1: Klinkenberg-corrected
20 permeability as a function of quartz % volume, B2: Brine permeability as a function of
21 quartz % volume.

22

23 **Figure 9.** Measured klinkenberg-corrected permeability as a function of pore diameter
24 for the 3 recognised pore types: including nano-intercrystalline, micro-intercrystalline
25 and meso-intercrystalline pore systems.

26

27 **Figure 10.** Measured klinkenberg-corrected permeability as a function of the pore throat
28 size for 21 samples. The pore throat size has been calculated from the application of
29 the Washburn equation to the measured at threshold point on the respective capillary
30 pressure curve.

31

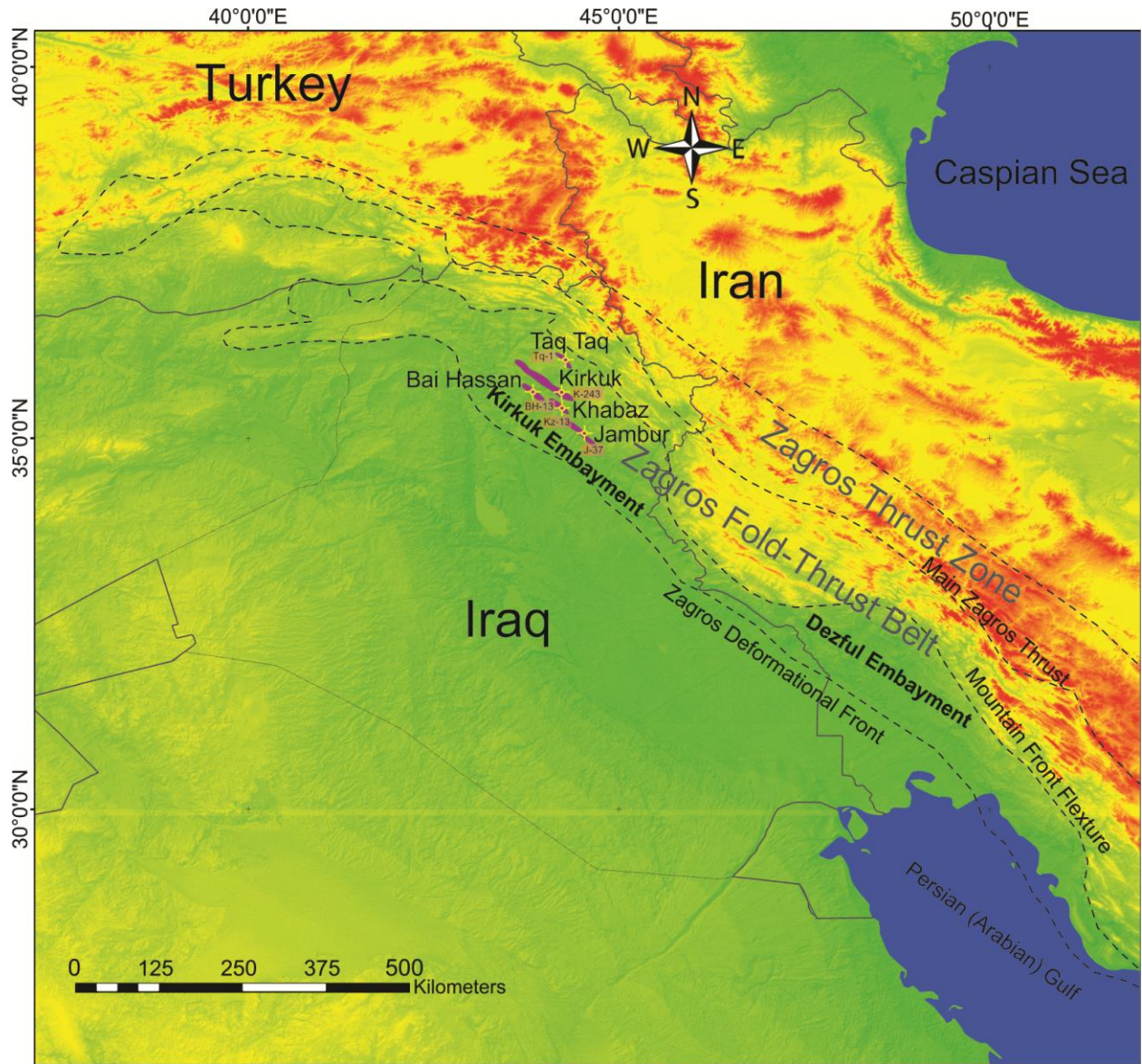
32

33

34

35

1



2 Figure 1

3

4

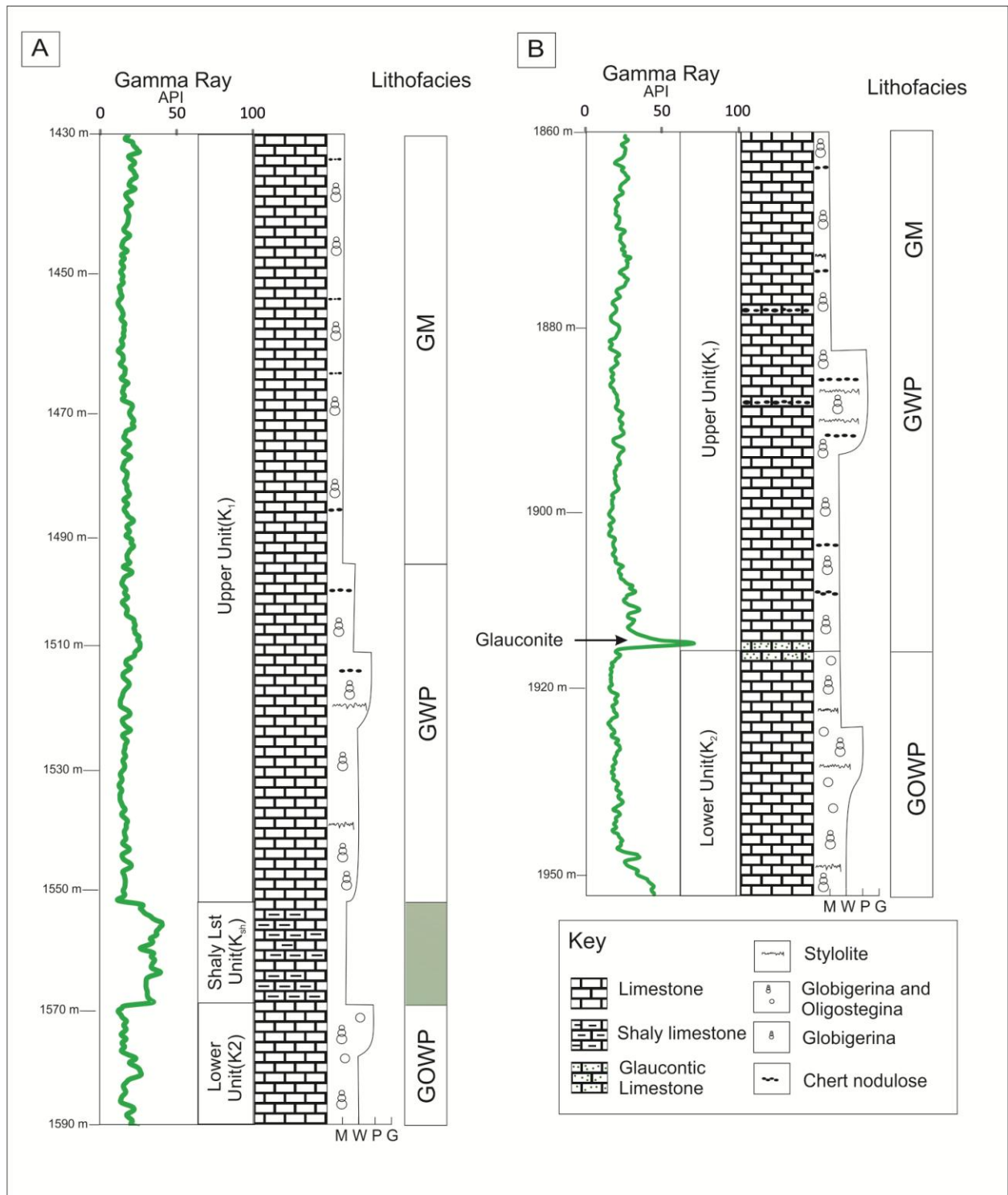
5

6

7

8

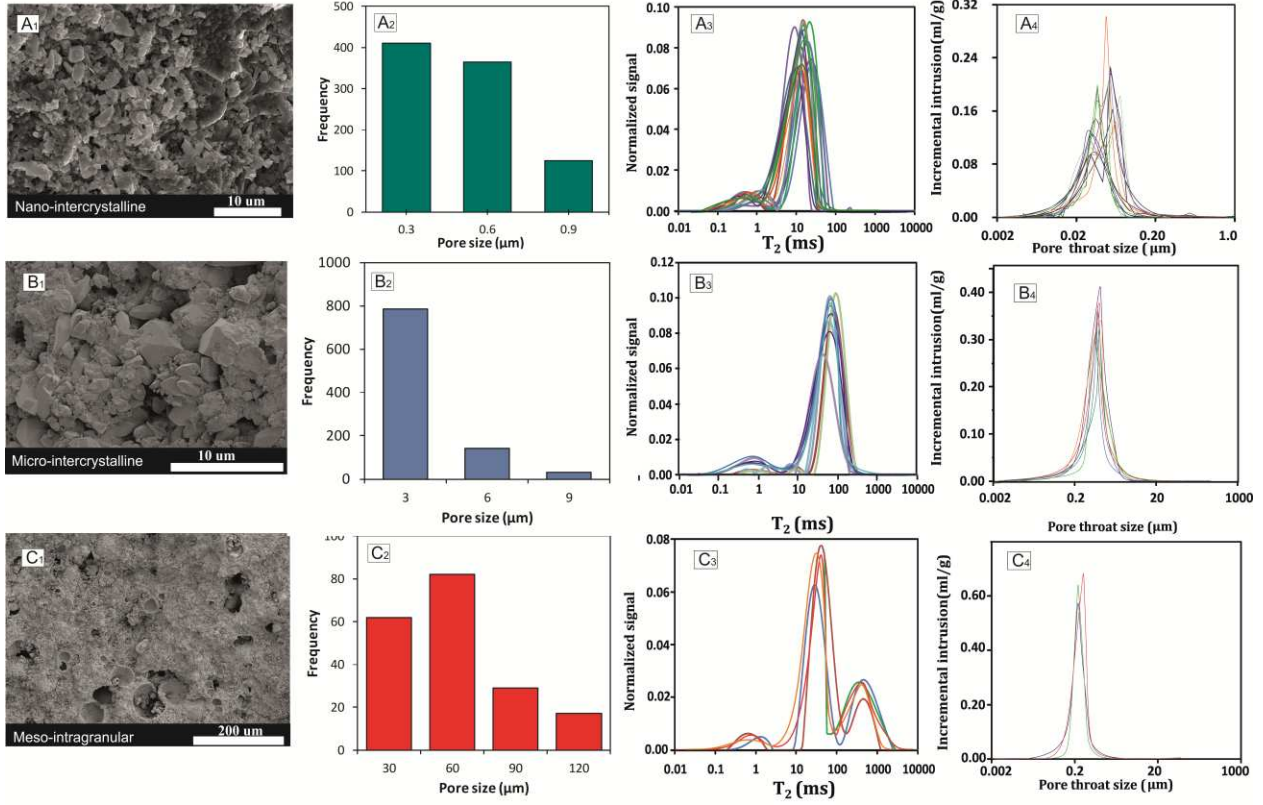
9



1 Figure 2

2

3



1 Figure 3

2

3

4

5

6

7

8

9

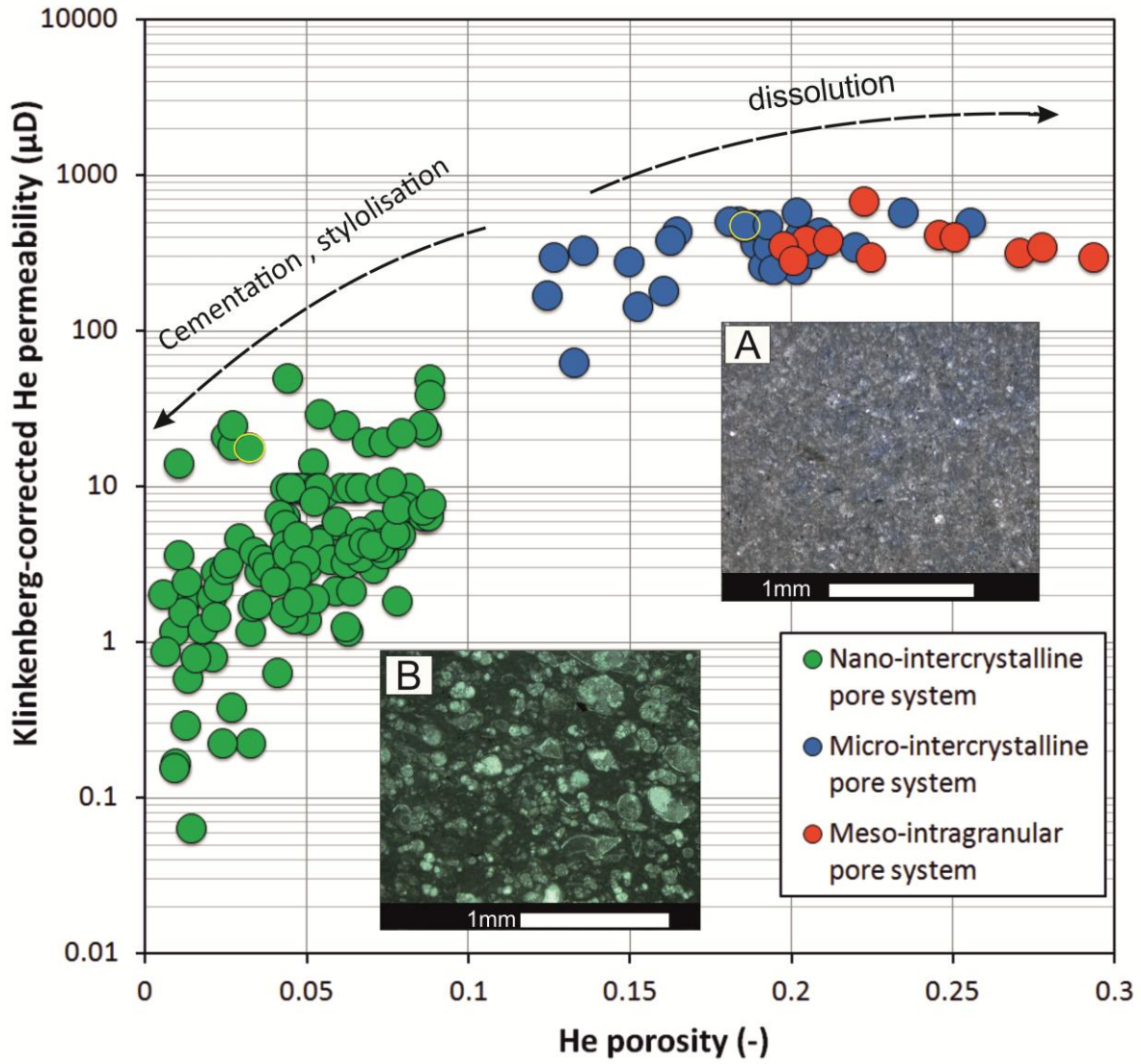
10

11

12

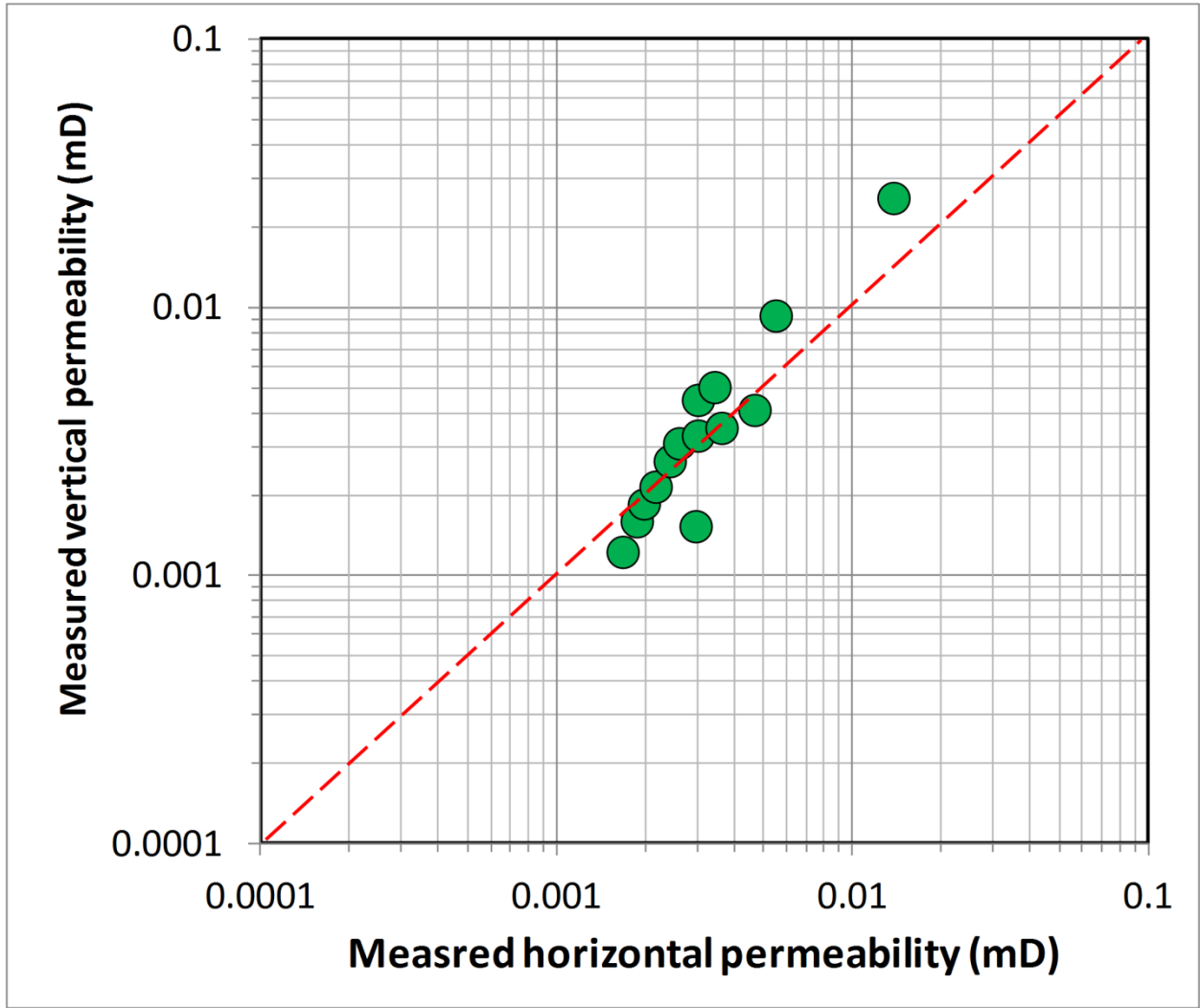
13

14



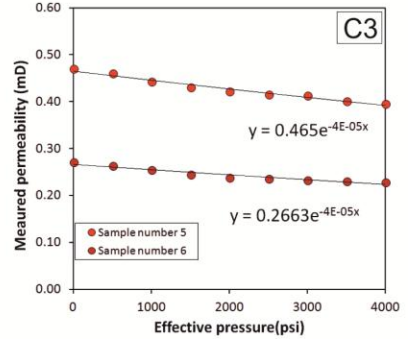
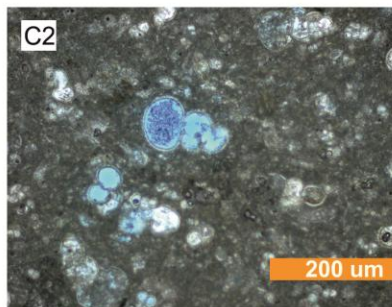
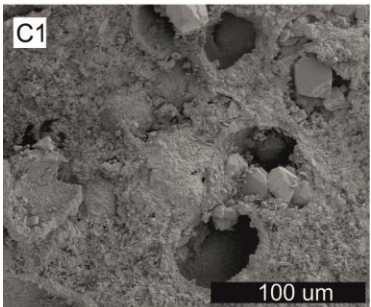
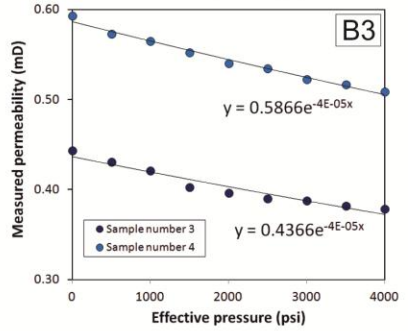
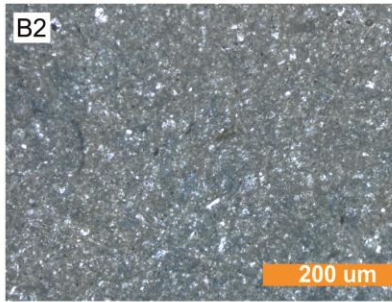
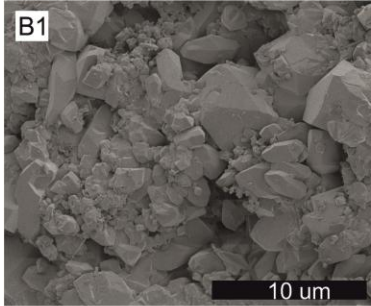
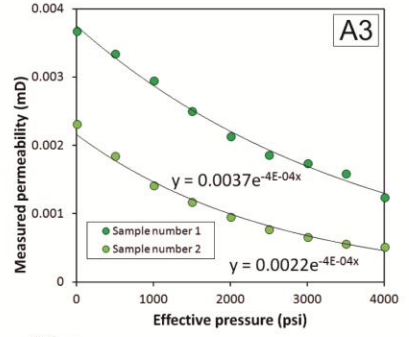
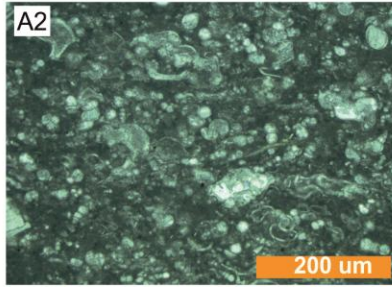
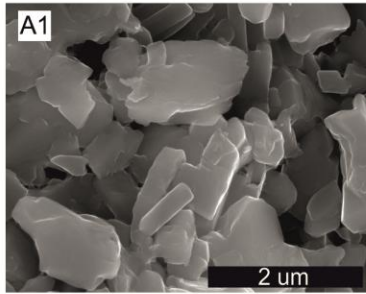
1 Figure 4

- 2
- 3
- 4
- 5
- 6
- 7
- 8
- 9



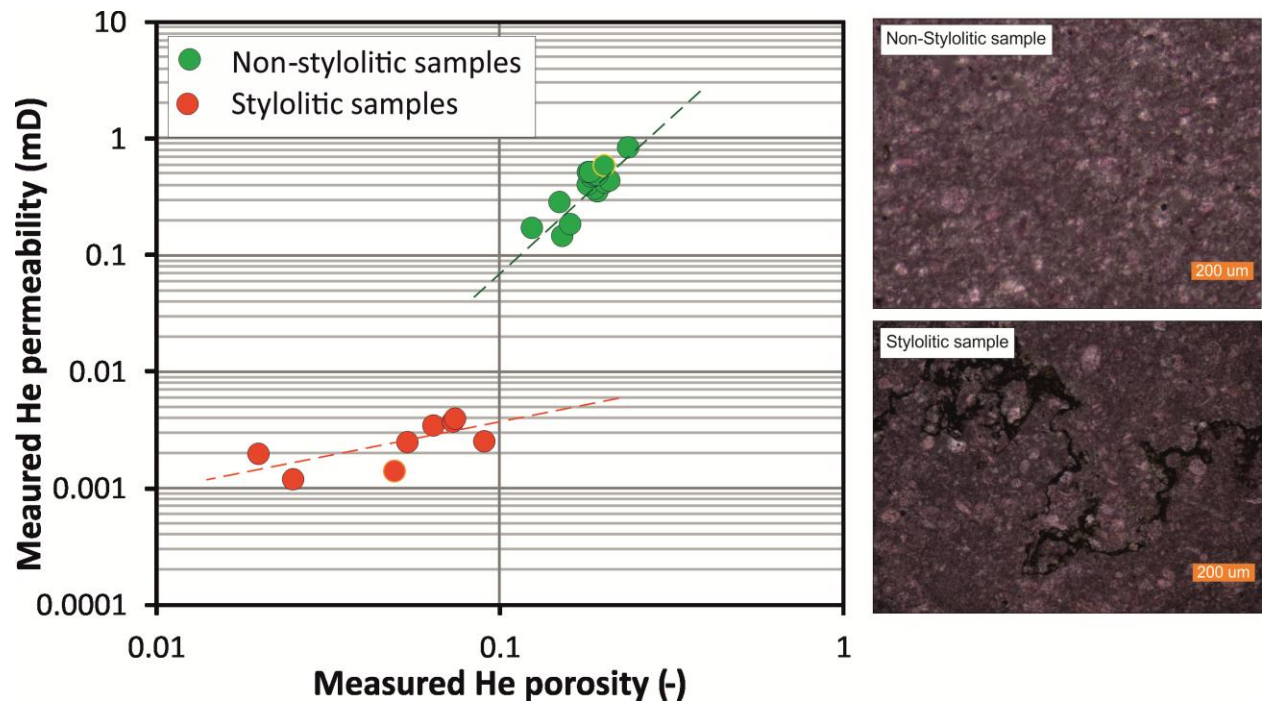
1 Figure 5

- 2
- 3
- 4
- 5
- 6
- 7
- 8
- 9
- 10



1 Figure 6

- 2
- 3
- 4
- 5
- 6
- 7
- 8
- 9
- 10
- 11



1 Figure 7

2

3

4

5

6

7

8

9

10

11

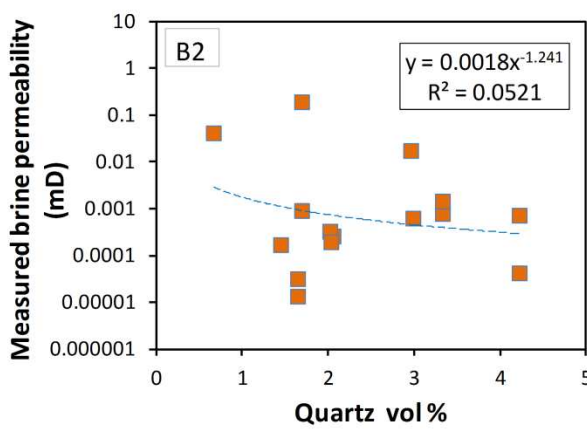
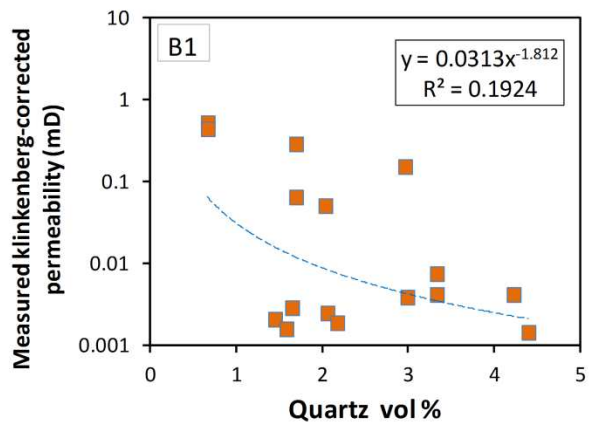
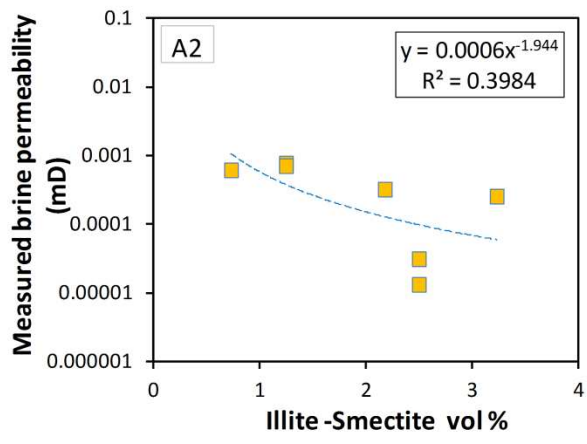
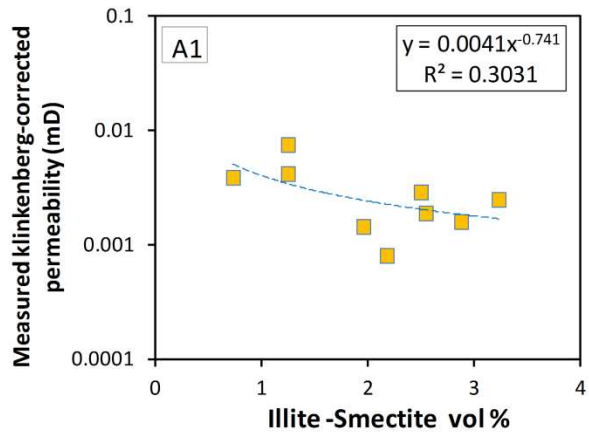
12

13

14

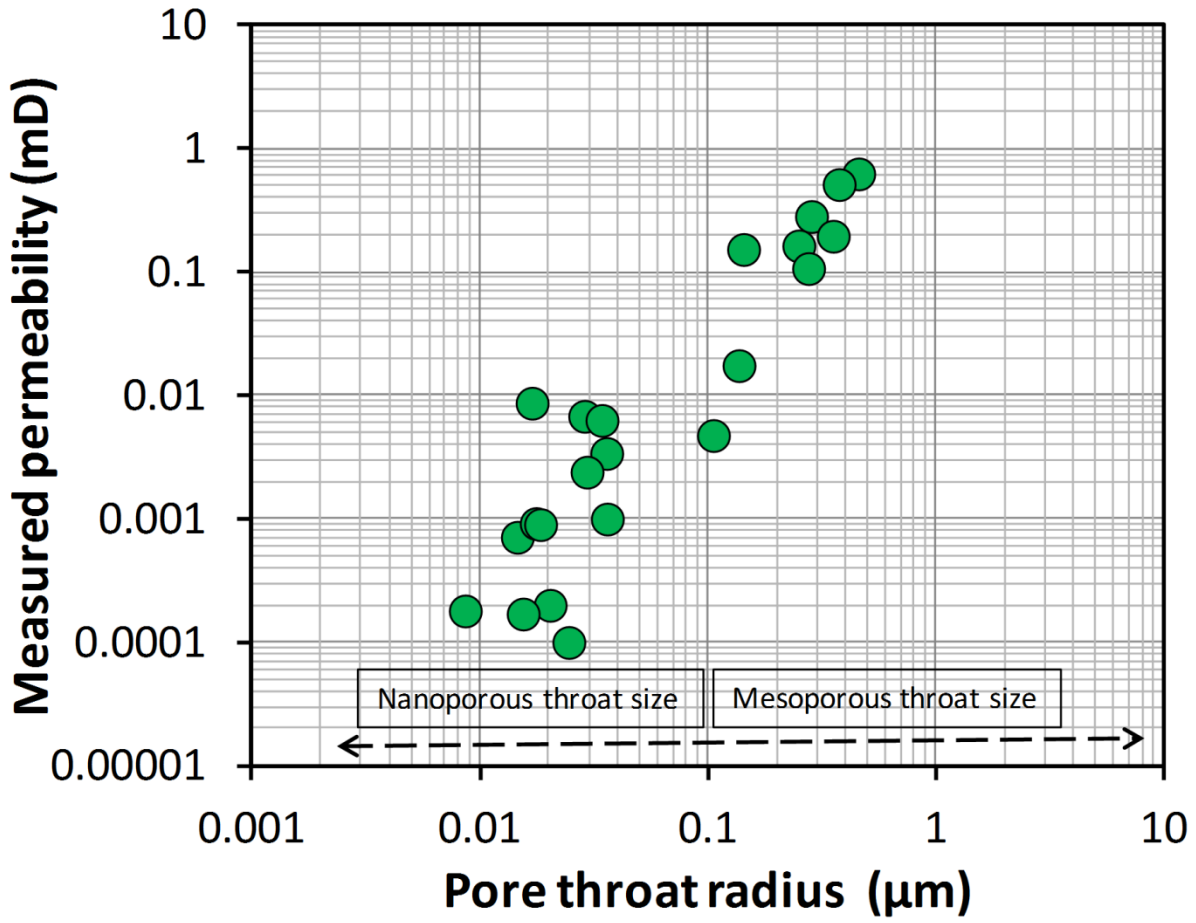
15

16



1 Figure 8

- 2
- 3
- 4
- 5
- 6
- 7
- 8
- 9
- 10
- 11
- 12
- 13



1 Figure 10